J. COMBIN. MATH. COMBIN. COMPUT. 127b (2025) 7925--7944

Journal of Combinatorial Mathematics and Combinatorial Computing
www.combinatorialpress.com/jcmcc

Combinatorial Press

# Optimized scheduling of off-grid wind power hydrogen production system considering battery and electrolyzer degradation

Ende Zong[1,✉], Chengxu Tang[2], Chunyang Qiu[1], Yan Dong[1]

[1] *School of Electrical Engineering, Hebei University of Technology, Tianjin, 300131, China*
[2] *Department of Electrical and Computer Engineering, Santa Clara University, 500 El Camino Real, Santa Clara, California, CA 95053, United States*

ABSTRACT
The development of off-grid wind power to hydrogen systems is crucial for promoting renewable energy, reducing dependence on fossil fuels, and achieving sustainable energy development. However, the volatility of wind power can lead to problems such as shortened service life of batteries and electrolyzers. This study proposes an optimized scheduling strategy for off-grid wind power hydrogen generation systems, considering the degradation of batteries and electrolyzers, with a focus on the impact of battery state of charge (SOC) overrun and electrolyzer overload on system operation. A voltage degradation model for electrolyzers was established by analyzing different operating conditions, aiming to improve utilization capacity and reduce degradation costs. Additionally, a degradation model for energy storage batteries was developed, considering factors such as cycle depth, cycle number, and SOC overrun, to optimize charging and discharging operations, extend battery life, and reduce degradation costs. The effectiveness of the proposed scheduling strategy was verified through detailed simulation analysis, demonstrating improved wind power consumption capacity, slowed degradation of batteries and electrolyzers, and ultimately enhanced economic benefits for the system.

*Keywords:* wind-to-hydrogen conversion, optimal scheduling, electrolyzer degradation, battery degradation, mongoose optimization algorithm

## 1. Introduction

The current world energy crisis has pushed the energy industry into a new phase of clean energy transformation, and renewable energy is gradually replacing existing fossil energy as the dominant

✉ Corresponding author.
*E-mail address:* 202221401077@stu.hebut.edu.cn (E. Zong).
Received 12 February 2024; Revised 15 April 2024; Accepted 25 November 2024; Published Online 16 April 2025.
DOI: 10.61091/jcmcc127b-433

energy source. In order to realize the goal of zero carbon emission in the global energy system, countries are actively researching and developing clean energy-related technologies, including renewable energy system technologies such as solar energy, wind energy, biomass energy, geothermal energy, and new energy system technologies such as advanced nuclear energy and hydrogen energy [1-3]. In the process of energy system development towards decarbonization and carbon-free, hydrogen energy has become an important direction of clean energy development, providing an important solution to realize zero carbon emission of energy [4-5]. Hydrogen energy, as a secondary energy source, is a carrier capable of storing energy and releasing it at the right time, and is gradually developing into an important carrier for energy transition [6]. The development of large-scale hydrogen energy industry can promote the national energy decarbonization process, accelerate the realization of the “dual-carbon” goal [7].

The development and application of hydrogen generation technology from renewable energy sources, such as wind power, provides an important solution for realizing zero-carbon energy emissions. Off-grid wind power hydrogen production system has the advantages of high reliability and flexibility, which is the best way to realize the efficient utilization of wind energy and large-scale low-cost production of hydrogen energy [8-9]. Since off-grid wind power hydrogen production system does not depend on the power grid, it has better ability to cope with situations such as power outages, and the system design is more flexible, so it can provide a reliable supply of electricity and hydrogen energy to remote areas that lack power grid resources [10-12]. Among them, the electrolyzed water hydrogen generator is the core equipment of the system, and its dynamic characteristics are crucial for the development of the control strategy of the wind power hydrogen generation system [13-14]. In renewable energy hydrogen production systems, there are two configurations of electrolyzer capacity, one using a large-capacity electrolyzer for hydrogen production and the other using multiple small-capacity electrolyzers for hydrogen production [15]. Although the former has a large capacity, high production efficiency and easy operation, the latter has a wider load operating range and higher flexibility, reliability and scalability, which is conducive to improving economic efficiency and resource utilization [16-19]. With the application of hydrogen production equipment on a large scale, it has become an inevitable trend to realize the integration and modularization of multiple equipment, and the optimization of the electrolyzer control strategy has become a much-anticipated research topic.

Since wind power generation as the input power of the hydrogen production system has volatility and uncertainty, this will lead to frequent start and stop of the electrolyzer, which will not only reduce its own service life, but also lead to a decrease in the amount of hydrogen production, and even affect the purity of the product hydrogen and the concentration of hydrogen in the oxygen, which in turn affects the safety of the entire electrolytic water hydrogen production system. Therefore, to improve the ability of the electrolyzer to adapt to wide power fluctuations, increase the hydrogen production of the hydrogen production system, as well as to extend its service life, you can optimize the diaphragm material to improve the performance of the electrolyzer. Peng, W. et al. investigated the operational characteristics of proton exchange membrane (PEM) electrolytic cell in wind power hydrogen production system, and clustered the wind power output data by self-organized mapping neural network algorithm to provide theoretical reference for the performance degradation of PEM electrolytic cell under wind fluctuation conditions [20]. Zhao, D. et al. analyzed the dynamic response process of high temperature proton exchange membrane (HT-PEMEC) electrolyzer through a two-dimensional multi-physics model and optimized the electrolyzer control strategy accordingly to guarantee fast and safe electrolyzer operation [21]. Guo, Y. et al. constructed a hybrid electrolyzer by combining the advantages of proton exchange membrane and alkaline electrolyzer, and at the same time formulated a hybrid electrolyzer system control scheme based on the start-stop characteristics of its operation process and the variation of HTO concentration in order to optimize the adaptability to power fluctuation and the economic efficiency of the operation of the hybrid electrolyzer [22].

Since the research on electrolyzer materials and new materials is a long-term and complex process, it is difficult to meet the demand for electrolyzer to adapt to wide power fluctuations in the short term, while changing the capacity configuration of electrolyzer for hydrogen production system and optimizing the control strategy of electrolyzer are worth considering in the short term. Fang, R. et al. designed a wind-hydrogen integrated energy system integrated supercapacitor for the impact of wind power fluctuation on hydrogen production and its own safety in alkaline electrolyzer to reduce the number of starting and stopping of the electrolyzer by absorbing transient fluctuation of wind power input while controlling the wide power fluctuation by using an adaptive control strategy to realize the wind power fluctuation smoothing [23]. Wang, X. et al. considered the minimum hydrogen production power constraint of the electrolyzer and used a priority scheduling method to allocate the renewable energy input power to different electrolyzers to break the minimum operating power threshold in order to reduce the number of electrolyzer starts and stops [24]. Li, Y. et al. compared two control optimization strategies in a multi-electrolyzer wind-powered hydrogen generation system, and compared to the equal-power strategy, the power distribution and working time between the multiple electrolyzers under the doctor-sharing strategy are more balanced, which reduces the safety risk of the power system and significantly improves the energy efficiency and reliability of commercial alkaline water electrolyzers [25]. Zheng, Y. et al. established an electrolyzer model integrating the influencing factors of load variation, start-stop cycling, and thermal management to enhance the efficiency of managing multiple electrolyzers in a wind-hydrogen system, and proposed a control strategy based on rolling optimization, which improves the system's hydrogen production efficiency and economic benefits [26].

In addition, some scholars have introduced optimization algorithms into the multi-electrolyzer switching scheduling strategy, which is conducive to further improving the performance of the hydrogen production system. Huang, W. et al. proposed an optimal scheduling strategy for hydrogen production from electrolytic water in microgrids based on an improved beluga optimization algorithm, which can effectively achieve the optimal utilization of electrolysis tanks by optimizing the mathematical model in terms of the economic cost, the system operating rate, and the hydrogen demand [27]. Niu, M. et al. used the non-dominated sorting genetic algorithm (NSGA-II) and entropy value method to optimize the control strategy of alkaline electrolyzer operation under multiple constraints, which greatly strengthened the dynamic hydrogen production efficiency of the system under wind power supply [28]. Liang, T. et al. applied the Pelican Optimization Algorithm (POA) to the multi-electrolyzer switching scheduling strategy for wind power hydrogen production system, which can obtain smooth power fluctuation under different wind scenarios, significantly reduce the electrolyzer start-stop cycle, and then improve the overall performance of the wind power hydrogen production system [29]. The above studies have proposed corresponding optimization strategies for the economic and reliability objectives of renewable energy hydrogen production systems with full consideration of the battery and electrolyzer degradation phenomena, but there are fewer studies oriented to off-grid wind power hydrogen production systems, and further studies are expected to be carried out.

For an off-grid wind power hydrogen generation system, this study proposes an optimized scheduling strategy considering the degradation of the battery and electrolyzer, with special attention to the impact of battery SOC overrun and electrolyzer overload on the system operation. By analyzing different operating conditions, an electrolyzer voltage degradation model was established to improve the utilization capacity and reduce the degradation cost. This study establishes a degradation model for energy storage batteries by considering factors such as cycle depth, cycle number, and SOC overrun to optimize the charging and discharging operations, extend the battery life, and reduce the degradation cost. The effectiveness of the proposed scheduling strategy was verified through a detailed simulation analysis. The results show that the strategy can improve the wind-power consumption capacity, effectively slow the degradation of the battery and electrolyzer, and ultimately improve the economic benefits of the entire system.

## 2. Structure of Off-Grid Wind Power Hydrogen Production System and Degradation Model of Batteries and Electrolyzer

An off-grid wind power hydrogen production system can enhance the utilization efficiency of renewable energy and mitigate the volatility and intermittency of renewable energy sources. This system is widely implemented in regions distant from the power grid or in areas with unstable power supply. Figure 1 illustrates the structure of the off-grid hydrogen-production system used in this study. The system primarily comprises wind turbines, battery packs, and electrolyzers. When the wind turbine output power is high, energy storage batteries can be employed to absorb excess electricity, thereby balancing the system power. Conversely, when the wind turbine output power is low, the energy storage battery can discharge the stored energy to compensate for insufficient electrical energy, ensuring continuous and stable operation of the electrolyzer and facilitating hydrogen gas production.

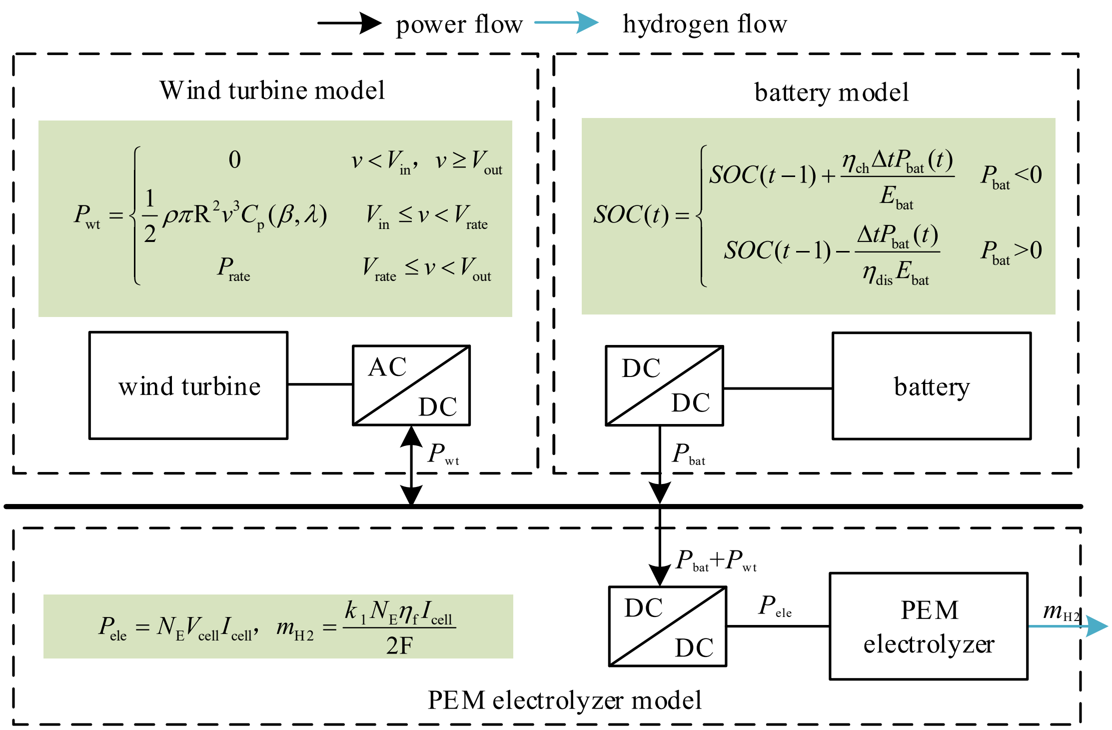


**Fig. 1.** Off-grid wind power hydrogen generation system structure

The parameters of the wind turbine model depicted in the figure are as follows: $v$ is the input wind speed, $V_{in}$ is the inlet wind speed, $V_{out}$ is the outlet wind speed, $V_{rate}$ is the rated wind speed, $\rho$ is the air density, $R$ is the wind turbine blade radius, $C_p$ is the wind energy utilization coefficient, and $P_{rate}$ is the rated power of the wind turbine. The parameters of the energy storage battery model are as follows: $\eta_{ch}$, $\eta_{dis}$ is the battery charging and discharging efficiency, $\Delta t$ is the charging and discharging duration, $E_{bat}$ is the battery capacity, and $SOC$ is the battery state of charge. The parameters of the electrolyzer model are as follows: $m_{ele}$ hydrogen yield, $k_1$ is the electric hydrogen conversion coefficient, $F$ Faraday constant;, $N_E$ number of electrolyzers, $\eta_f$ Faraday efficiency of the electrolyzer and $I_{cell}$ is, electrolyzer current.

### 2.1. Degradation model of energy storage battery

The depth of charge and discharge (DOD) of energy storage batteries influences their degradation rate, with a higher DOD correlating with accelerated degradation. Conversely, a lower DOD results in slower degradation. The relationship between the total number of cycles N and the DOD can be characterized by a fourth-order function.

$$N(d) = -3278d^4 - 5d^3 + 12823d^2 - 14122d + 5112 \tag{1}$$

where, $d$ is the depth of charge and discharge of the battery.

Owing to the high stochasticity of wind-power fluctuations, it is challenging to quantify the number of cycles. Consequently, the cycles at different DOD were equal to the number of full charge and discharge.

$$n(d) = \frac{C_{NT}(d)N(1)}{N(d)} \tag{2}$$

where, $CNT$ ($d$) represents whether it is a full cycle or a half cycle when the depth of charge and discharge is d, with a full cycle value of 1 and a half-cycle value of 0.5, $N$ (1) is the maximum number of cycles for the battery to be fully charged and discharged. $N$ (d) represents the number of times the energy storage battery completes one charge and discharge, equivalent to the full charge and discharge at a depth of d.

Assuming that the battery undergoes m charge and discharge cycles per day, the calculation formula for the operating life $T_d$ of the energy storage battery is as follows:

$$N_d = \sum_{i=1}^{m} n_i(d_i) \tag{3}$$

$$T_d = \frac{N_d}{N(1)} \tag{4}$$

where, $T_d$ is used to evaluate the degradation of the energy-storage battery SOC between 0 and 1.

The degradation of the normal operating range of the battery state of charge (SOC) was previously analyzed; however, in the actual charging and discharging process, minor overcharging (110% SOC) and overdischarging (-8% SOC) of lithium-ion batteries are unavoidable, and the extent of degradation caused by such overcharging and overdischarging remains within a manageable range. Consequently, to optimize the balance between the capacity utilization and degradation rates of energy-storage batteries, a degradation model for battery overcharging and overdischarging was developed.

$$T_{\text{over}} = \begin{cases} A_0 \exp(-C / t_0) + y_0 & SOC<0 \\ a + bC & SOC>1, C<1 \\ c & SOC>1, C \geq 1 \end{cases} \tag{5}$$

where,$C$ represents the battery charging and discharging rates, $P_{bat}$ greater than 0 indicates battery discharge, and $P_{bat}$ less than 0 indicates battery charging. $A_0$, etc. are fitting parameters.

### 2.2. Electrolyzer degradation model

The continuous operation of an electrolyzer can result in a reduction in its operational lifespan, and most studies indirectly reflect this decline through experimental measurements of voltage changes in the electrolyzer. When the voltage of the electrolyzer reaches the maximum operating voltage threshold, the electrolyzer must be replaced to ensure the stable operation of the system.

$$V_{\text{cell}} = V_{\text{oc}} + V_{\text{act}} + V_{\text{ohm}} \tag{6}$$

$$V_{\mathrm{act}}=\frac{RT}{a_{\mathrm{A}}zF}\operatorname{arcsin}\mathrm{h}(\frac{j}{2j_{0,\mathrm{A}}})+\frac{RT}{a_{\mathrm{C}}zF}\operatorname{arcsin}\mathrm{h}(\frac{j}{2j_{0,\mathrm{C}}}) \tag{7}$$

$$V_{\mathrm{ohm}}=j(R_{\mathrm{el}}+R_{\mathrm{mem}}+R_{\mathrm{Ti}}) \tag{8}$$

where, $z$ is the number of electrons involved in the reaction, $J_0$ is the exchange current density, $R_{\mathrm{el}}$ is the electrode resistance, $R_{\mathrm{mem}}$ is the proton exchange membrane ohmic resistance, $R_{\mathrm{Ti}}$ is the bipolar plate titanium oxidation resistance, and $\alpha_{\mathrm{A}}$ and $\alpha_{\mathrm{C}}$ are the charge-transfer coefficients at the anode and cathode, respectively.

Under low, high, and overload power conditions, the electrolyzer membrane tends to decrease in thickness. As the membrane thickness decreased, the membrane resistance increased, resulting in a corresponding increase in overvoltage within the electrolyzer. This relationship can be expressed as follows:

$$\Delta V_{\mathrm{mem}}=j\Delta R_{\mathrm{mem}} \tag{9}$$

$$R_{mem}=\frac{{\delta_{0,\mathrm{mem}}}^{2}}{k_{0}\delta_{\mathrm{mem}}} \tag{10}$$

$$\delta_{\mathrm{mem}}=\delta_{0,\mathrm{mem}}-\frac{v_{\mathrm{Rr}}}{\lambda_{\mathrm{f}}\rho_{\mathrm{M}}} \tag{11}$$

where, $\delta_{\mathrm{mem}}$, $\delta_{0,\mathrm{mem}}$ represent the current membrane thickness and initial membrane thickness, respectively; $v_{\mathrm{Rr}}$ is the fluoride release rate; $\lambda_{\mathrm{f}}$ is the fluorine content in the PEM; $\rho_{\mathrm{M}}$ is the density of the PEM membrane; $K_0$ is the initial membrane conductivity.

As the electrolyzer voltage increased, the fluoride release rate gradually increased. The accelerated thinning of the electrolyzer membrane exacerbated the performance degradation of the electrolyzer. The fluoride release rate was calculated as follows:

$$v_{\mathrm{Rr}}=A_{1}\frac{\Delta P_{\mathrm{O_2}}}{P_{0}}\frac{\delta_{0,\mathrm{mem}}}{\delta_{\mathrm{mem}}}\mathrm{e}^{(\frac{\alpha_{\mathrm{eq}}F}{RT}V\mathrm{cell})}\mathrm{e}^{(-\frac{E_{\mathrm{a}}}{R}(\frac{1}{T}-\frac{1}{T_{0}}))} \tag{12}$$

where, $\Delta P_{\mathrm{O2}}$ is the oxygen partial pressure difference at the electrolyzer inlet, $P_0$ is the reference pressure of the electrolyzer, $a_{\mathrm{eq}}$is the equivalent transfer coefficient, $E_{\mathrm{a}}$ is the activation energy, $T_0$ is the reference temperature, $A_1$ is an adjustable constant.

Under high-power operating conditions, the degradation rate of the electrolyzer exceeded that observed under low-power conditions, which is attributable to factors other than membrane degradation. During prolonged exposure to high current density conditions, the bipolar plate and porous transport layer (PTL) undergo accelerated oxidation, resulting in an increase in the ohmic resistance. Consequently, the electrolyzer exhibited a more rapid degradation trend during high-power operations.

$$\Delta V_{\mathrm{Ti}}=jR_{\mathrm{Ti}} \tag{13}$$

$$R_{\mathrm{Ti}}=k_{\mathrm{ohm}}\sum_{t=1}^{t_{\max}}\max(0,j-\varepsilon_{2}) \tag{14}$$

where $k_{\mathrm{ohm}}$ represents the oxidation rate and $\varepsilon_2$ is the threshold for a high current density.

The electrolyzer possesses a 150% overload capacity, which is advantageous for enhancing the absorption and utilization of renewable energy sources such as wind power. However, under overload conditions, the electrolyzer membrane thickness decreases at an accelerated rate, resulting in an increased ohmic overvoltage. Furthermore, when an electrolyzer operates under overload conditions for more than 2 h, its internal structure or function may sustain irreversible damage. Consequently, to ensure safe operation and long-term stability of the electrolyzer, it is imperative to impose limitations on its continuous overload duration.

$$T_{\text{conover}} \leq 2 \tag{15}$$

Fluctuations in the electrolyzer potential primarily contribute to the degradation of the catalysts, particularly those situated on the anode. This degradation subsequently resulted in a decrease in the catalytic activation performance, leading to a reduction in the exchange current density.

$$\Delta V_{\text{pt}} = V_{\text{act}}(j, \Delta j_0) \tag{16}$$

$$\ln\left(\frac{j_0^{'}}{j_0}\right) = \left(\frac{C_{\text{cl}}}{C_0}\right) \tag{17}$$

$$C_{\text{cl}} = C_0 - (k_{\text{dis}} - k_{\text{rdp}}) \sum_{t=1}^{t_{\max}} \max(0, (j_{t+1} - j_t) - \varepsilon_1) \tag{18}$$

where, $\Delta V_{\text{pt}}$ represents the amount of voltage degradation caused by catalyst degradation; $C_{\text{cl}}$ catalyst content; $C_0$ is the initial catalyst content; $\varepsilon_1$ is the threshold for potential fluctuations; $J_0$ 'is the degraded exchange current density; $J_0$ exchange current density; $\Delta\ j_0$ is the amount of exchange current density degradation; $K_{\text{rdp}}$ redeposition coefficient; $K_{\text{dis}}$ is the solubility coefficient.

During the startup and shutdown processes of the electrolyzer, the generation of reverse current accelerates the corrosion of carbon-based electrode materials, thereby exacerbating the degradation of the electrolyzer performance. The voltage degradation model of the electrolyzer based on the start-stop conditions is as follows:

$$\Delta V_{\text{st}} = k(S_{\text{on}} + S_{\text{off}}) \quad S_{\text{on}} \geq 1 \text{or} S_{\text{off}} \geq 1 \tag{19}$$

$$\begin{cases} S_{\text{on}} = S_{\text{on}} + 1 & P_{\text{ele}}(t\text{-}1) = 0 \ , P_{\text{ele}}(t) \geq P_{\text{ele,min}} \\ S_{\text{off}} = S_{\text{off}} + 1 & P_{\text{ele}}(t\text{-}1) \geq P_{\text{ele,min}} \ , P_{\text{ele}}(t) = 0 \end{cases} \tag{20}$$

where,$\Delta V_{\text{st}}$ represents the voltage degradation of the electrolyzer caused by the start–stop operation, $S_{\text{on}}$ is the daily start-up frequency of the electrolyzer, $S_{\text{off}}$ is the daily shutdown frequency of the electrolyzer, $P_{\text{ele}}$ (t) is the power of the electrolyzer at time $t$, $P_{\text{ele, min}}$ is the lower limit of the operating power of the electrolyzer, $k$ is the degradation coefficient for starting and stopping the electrolyzer.

The total voltage degradation of the electrolyzer is calculated using the following equation:

$$\Delta V_{\text{d}} = \Delta V_{\text{mem}} + \Delta V_{\text{Ti}} + \Delta V_{\text{pt}} + \Delta V_{\text{st}} \tag{21}$$

When the electrolyzer degradation voltage reaches a predetermined threshold, replacement becomes necessary. Consequently, minimizing voltage degradation in the electrolyzer extends its operational lifespan and enhances the economic viability and sustainability of the system.

## 3. Optimized scheduling of off-grid wind power hydrogen production system considering electrolyzer and battery degradation

In the off-grid wind power hydrogen production system, to ensure the hydrogen production of the system while reducing the degradation rate of the electrolyzer and battery, an optimization scheduling model is constructed by selecting objective functions such as hydrogen production revenue, electrolyzer voltage degradation cost, and energy storage battery degradation cost.

### *3.1. Objective function*

The primary objective of a hydrogen production system is to optimize the utilization of renewable energy by decomposing water into hydrogen via an efficient electrolysis process. Consequently, the maximization of hydrogen production yield was selected as the objective function, as represented by the following equation:

$$C_{\mathrm{H2}} = \frac{k_1 N_{\mathrm{E}} \eta_{\mathrm{f}} I_{\mathrm{cell}}}{2\mathrm{F}} c_{\mathrm{h2}} \tag{22}$$

where, $c_{h2}$ represents the price of hydrogen gas.

The electrolyzer, as the primary component of electrohydrogen coupling, is susceptible to input power fluctuations during extended operation, which results in accelerated degradation. Consequently, the electrolyzer degradation cost was selected as the optimization objective of the scheduling strategy.

$$C_{\mathrm{V}} = \frac{\sum_{t=1}^{T} \Delta V_{\mathrm{d}}}{\Delta V_0} c_{\mathrm{v}} \tag{23}$$

where, $c_{\mathrm{v}}$ is the cost of replacing the electrolyzer, and $\Delta V_0$ is the maximum degradation voltage of the electrolyzer.

Considering the State of Charge (SOC) over the limit of operation to enhance the capacity utilization of energy storage batteries, and with the aim of mitigating battery degradation, the degradation cost of energy storage batteries is selected as the objective function, as represented by the following equation:

$$\Delta B_{\mathrm{d}} = \begin{cases} T_{\mathrm{d}} & 0 \le SOC \le 1 \\ T_{\mathrm{over}} & 1 \le SOC \le 1.1, -0.08 \le SOC < 0 \end{cases} \tag{24}$$

$$C_{\mathrm{Bd}} = \Delta B_{\mathrm{d}} c_{\mathrm{bat}} + c_{\mathrm{bat,main}} (P_{\mathrm{bat}}) \Delta t \tag{25}$$

where, $c_{\mathrm{bat}}$ is the investment cost of the battery and $c_{\mathrm{bat,main}}$ is the unit maintenance cost of the battery.

Considering an off-grid hydrogen production system designed to maximize wind power utilization, the objective function incorporates the cost of wind curtailment, as represented by the following equation:

$$C_{\mathrm{loss}} = P_{\mathrm{loss}} c_{\mathrm{loss}} \quad P_{\mathrm{loss}} > 0 \tag{26}$$

where, $P_{\mathrm{loss}}$ is the system wind power loss.

Considering the above costs and benefits, net operating income can be obtained as follows:

$$f = C_{\mathrm{H2}} - C_{\mathrm{V}} - C_{\mathrm{Bd}} - C_{\mathrm{loss}} \tag{27}$$

### 3.2. Constrained condition

Power balance constraints and wind turbine constraints.

$$P_{\mathrm{ele}}(t) = P_{\mathrm{wt}}(t) + P_{\mathrm{bat}}(t) - P_{\mathrm{loss}}(t) \tag{28}$$

$$P_{\mathrm{wt,min}} \le P_{\mathrm{wt}}(t) \le P_{\mathrm{wt,max}} \tag{29}$$

where, $P_{\mathrm{wt,\,max}}$, $P_{\mathrm{wt,\,min}}$ are the upper and lower limits of system input wind power, respectively.

Energy storage battery constraints.

$$P_{\mathrm{bat,min}} \le P_{\mathrm{bat}}(t) \le P_{\mathrm{bat,max}} \tag{30}$$

$$SOC_{\mathrm{min}} \le SOC(t) \le SOC_{\mathrm{max}} \tag{31}$$

$$SOC(T) = SOC_{\mathrm{opt}} + 0.1 \tag{32}$$

where, $P_{\mathrm{bat,\,max}}$ and $P_{\mathrm{bat,\,min}}$ are the upper and lower limits of the power interaction of the energy storage battery; $SOC_{\mathrm{max}}$ and $SOC_{\mathrm{min}}$ are the upper and lower limits of the state of charge of the energy storage battery, respectively; and Equation (32) represents the periodic operation limit of the energy storage device, ensuring its ability to operate periodically.

Constraints on the operation of electrolyzers.

$$P_{\mathrm{ele,min}} \le P_{\mathrm{ele}}(t) \le P_{\mathrm{ele,max}} \tag{33}$$

$$0 \le S_{\mathrm{on}} \le S_{on,\mathrm{max}} \tag{34}$$

$$0 \le S_{\mathrm{off}} \le S_{\mathrm{off,max}} \tag{35}$$

where, $P_{\mathrm{ele,\,max}}$ and $P_{\mathrm{ele,\,min}}$ are the upper and lower limits of the operating range of the electrolyzer, $S_{\mathrm{on}}$ is the daily startup frequency, $S_{\mathrm{on,\,max}}$ is the maximum daily startup frequency, $S_{\mathrm{off}}$ is the number of daily shutdowns, $S_{\mathrm{off,\,max}}$ is the maximum number of daily shutdowns.

# 4. Multistrategy improvement of mongoose optimization algorithm

The mongoose optimization algorithm employs a group search strategy for collaborative optimization among three groups of mongooses, which exhibits a rapid solving speed. This algorithm only requires the determination of population size and iteration times, demonstrating low sensitivity to parameters and high robustness in practical applications. Consequently, for the scheduling problem addressed in this study, the mongoose optimization algorithm was selected as the solution method. To further enhance the global search capability when addressing the problem in this study and mitigate minor power fluctuations caused by random space search, this paper presents an improved mongoose optimization algorithm, referred to as ECPS-DMO.

## *4.1. Multi strategy improvement of mongoose algorithm*

First, the conventional algorithm employs a standard random method for population initialization, resulting in initial population positions that are highly arbitrary and cannot ensure a uniform distribution throughout the solution space, consequently leading to a slow population search and insufficient diversity. In this study, the Latin hypercube sampling method was applied to initialize the original individual positions to enhance the global search capability and adaptive capacity of the algorithm.

The second improvement pertains to the convergence factor $r$ and $CF_{\text{new}}$, which demonstrate a nonlinear decrease from 1 to 0, with the curve maintaining a plateau during the initial iteration process. This algorithm effectively explored the entire search space.As the iterations progressed, the curve demonstrated rapid decay, leading to swift algorithm convergence. The convergence speed is enhanced in the early stages of optimization, whereas the convergence accuracy is improved in the later stages, as illustrated in equations (36)-(38).

$$CF_{\text{new}} = 1 - \sin\left(\frac{\pi}{2} \times \left(\frac{t}{T}\right)^2\right) \tag{36}$$

$$r = \cos\left(\frac{\pi}{2} * \left(\frac{t}{T}\right)^4\right) \tag{37}$$

$$x_i = \begin{cases} x_{\text{best}} * r - rand * \left(x_i - x_{\text{best}}\right) & rand > 0.5 \\ x_i + CF_{\text{new}} * phi * rand * [x_i - M] & rand \le 0.5 \end{cases} \tag{38}$$

where $x_{\text{best}}$ is the current global optimal position of the algorithm, *phi* is a random number uniformly distributed in [-1,1]; *Rand* is a random number from 0 to 1, $M$ is the latest sleep hill, $x_{\text{i}}$ is the location of individual i in the mongoose, $CF_{\text{new}}$ is the convergence factor of the reconnaissance team, $t$ is the current iteration count, $T$ is the maximum number of iterations.

The third improvement involves the proposal of a power grading strategy, taking into account the fluctuation in electrolyzer power and algorithm calculation rate, as illustrated in equations (39) and (40). This strategy categorizes the power of the PEM electrolysis cells into several discrete levels. When the algorithm population identified results close to the power classification value, it was designated as the classification value. This approach facilitates the mitigation of unstable results caused by random population search, enhances system computational efficiency, and reduces minor power fluctuations resulting from random spatial search, thereby improving overall system stability.

$$P_{\text{ele,min}} + \frac{a}{s}(P_{\text{ele,max}} - P_{\text{ele,min}}) \le P_{\text{ele}} \le P_{\text{ele,min}} + \frac{a+1}{s}(P_{\text{ele,max}} - P_{\text{ele,min}}) \tag{39}$$

$$P_{\mathrm{ele}}=\begin{cases}0, & P_{\mathrm{ele}}\le P_{\mathrm{ele,min}}\\ P_{\mathrm{ele,min}}+\dfrac{a}{s}(P_{\mathrm{ele,max}}-P_{\mathrm{ele,min}}), & P_{\mathrm{ele,min}}<P_{\mathrm{ele}}<P_{\mathrm{ele,max}}\\ P_{\mathrm{ele,max}}, & P_{\mathrm{ele}}\ge P_{\mathrm{ele,max}}\end{cases} \tag{40}$$

where, $s$ is the power rating number, which was set as 49 in this study. $a$ is a number between 0 and $s$-1.

### 4.2. Improve the optimization process of the mongoose algorithm

The multistrategy enhancement of the mongoose algorithm is predicated on the original algorithm, improving the convergence factor, global optimal value, and power-grading strategy. The solution flow of the improved algorithm is shown in Figure 2.

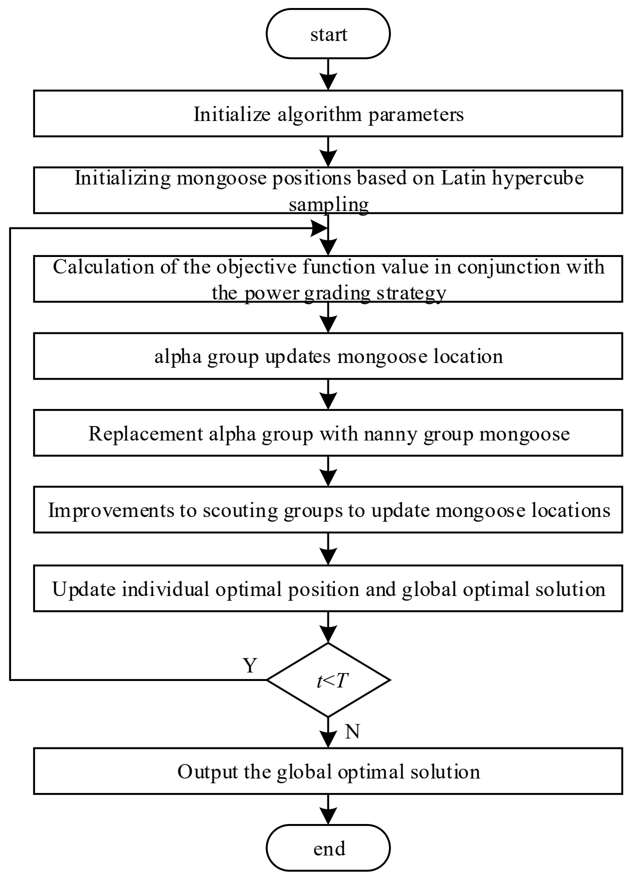


**Fig. 2.** Algorithm flow chart

Step1: Initialize the population size $n$, number of nanny groups $b_s$, number of alpha groups $n_a=n-b_s$, nanny exchange condition $L$, counter $C$, Initialization of mongoose positions based on Latin hypercubes and position of the individuals in the population represented by the battery power and input wind power , $x_i(i=1–n)$.

Step2: The power hierarchy strategy modifies the electrolyzer operating power, and subsequently calculates the net daily operating gain $fit_i=f(x_i)(i=1–n)$ for each individual in the population.

Step3: Individuals in the alpha group are selected as female alphas through roulette selection.

Step4: The female leader in the alpha group obtains new battery charging and discharging power and input wind power based on a randomized step.

Step5: Implement a power-grading strategy to calculate the net daily operating benefit $fit_i(t+1)$. If $fit_i(t+1)$ is superior to $fit_i(t)$, the optimal value is updated; otherwise, the current value is maintained. An increase in counter $C$ by 1.

Step6: Evaluate the nanny exchange condition for the mongoose in the alpha group. If $C>L$, the mongoose was exchanged between the alpha and nanny groups.

Step7: Convert the alpha group to the scout group, update the battery charging and discharging power and the input wind power according to the improved scout group search model (36)–(38), and calculate the corresponding daily operating net gain by incorporating a power classification strategy to update the global optimal solution.

Step8: Assess whether the termination condition is satisfied. If affirmative, proceed to Step9; otherwise, return to Step3.

Step9: Terminate the algorithm, and output the global optimal solution.

## 5. Case Study

To evaluate the feasibility of the proposed method, the system model incorporated a wind turbine with a rated capacity of 6 MW, PEM electrolysis cell with a rated power of 3.5 MW, and lithium battery with a rated capacity of 3.5 MWh. The parameters of each component in the off-grid wind power hydrogen production system are listed in Table 1 and Table 2.

**Table 1.** Parameters of electrolyzer and battery

| Parameter | Value | Parameter | Value |
|---|---|---|---|
| Electrolyzer efficiency | 0.75 | battery discharge efficiency | 0.93 |
| Maximum number of daily starts of the electrolyzer (times) | 3 | battery charging efficiency | 0.9 |
| Maximum number of daily stops in the electrolyzer (times) | 3 | battery power interaction upper limit(MW) | 7 |
| Higher power limit for electrolyzer operation(MW) | 3.5 | battery power interaction lower limit(MW) | -7 |
| Lower power limit for electrolyzer operation (MW) | 0.35 | Battery SOC initial value | 0.5 |
| Electrolyzer investment cost (yuan/kW) | 8000 | Battery investment cost(yuan/kWh) | 1500 |
| Hydrogen selling price (yuan/kg) | 45 | Wind abandonment cost(yuan/MW) | 350 |

**Table 2.** Parameters of electrolyzer degradation

| Parameter | Value | Parameter | Value |
|---|---|---|---|
| Anode exchange current density(A/cm2) | $2e^{-7}$ | Fluoride content (1) | 0.82 |
| Membrane conductivity(S/cm2) | 0.1603 | Anode catalyst content(mg/cm2) | 3 |
| Membrane density (g/cm3) | 20 | Charge transfer coefficient (1) | 2 |
| Membrane thickness(cm) | 0.02 | Contact resistance(Ω) | 0.03 |

In this algorithm, the key parameters were established as follows: population size of 40, number of iterations of 500, and time scale of optimal scheduling of 1 h. The data utilized were derived from actual measurements in the Hebei region, which ensured the accuracy and representativeness of the wind speed data.

Owing to the stochastic and fluctuating nature of wind power generation, it exhibits significant variation throughout the scheduling cycle. Under Typical Working Condition 1, wind power reaches its peak during the time periods 0~6h, 11~15h, and 23~24h, while it experiences troughs during the periods 7~9h and 16~21h. In contrast, Typical Case 2 demonstrates less wind power fluctuation, with a single substantial peak occurring from 17h to 24h, as illustrated in Figure 3.

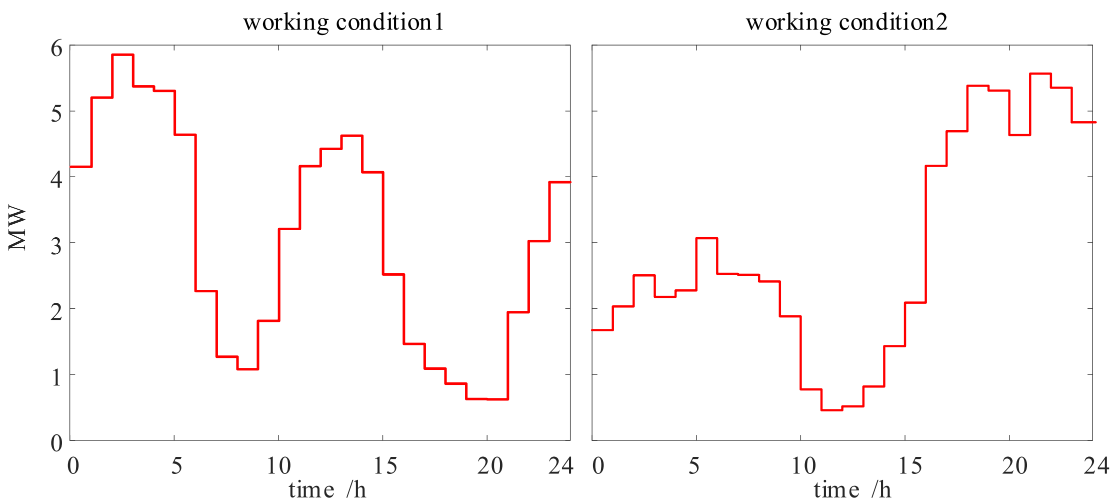


**Fig. 3.** Input wind power

Based on the aforementioned parameters and related indicators, four scheduling strategies are implemented to optimize the hydrogen production system. Strategy 1: The scheduling strategy does not consider electrolyzer overload and battery State of Charge (SOC) overrun; Strategy 2: the scheduling strategy does not consider electrolyzer overload but does consider battery SOC overrun; Strategy 3: the scheduling strategy considers electrolyzer overload but does not consider battery SOC overrun; Strategy 4: the scheduling strategy considers both electrolyzer overload and battery SOC overrun. The optimization results are subsequently presented.

Scheduling strategy 4 incorporates the overload operation capability of the electrolyzer and the overrun operation of the state of charge (SOC) of the energy storage battery. This approach ensures the utilization of the input wind power, mitigates wind curtailment, and enhances the economic efficiency of the system. System maintains power balance. The power distribution for each strategy is shown in Figure 4.

Upon examination of the figure, it is evident that the image exhibits symmetry above and below the 0 MW axis datum line. The region above the datum line encompasses the input wind power and battery discharge power, whereas the area below the datum line represents the hydrogen production power of the electrolyzer, the battery charging power, and the wind power abandonment.

In scheduling strategy 1, the potential for electrolyzer overload and battery state of charge (SOC) exceeding limits were not considered, resulting in significant wind power curtailment during 0-6 hours of operating condition 1 and 15-24 hours of operating condition 2.Under a scheduling strategy that solely considers the battery State of Charge (SOC) exceeding limits, although substantial wind power curtailment persists, operating energy storage batteries beyond the SOC limits during the 0-2 ,10-15 hour period of operating condition 1 and the 16-17 hour period of operating condition 2 can significantly enhance their peak-shaving capability and reduce the curtailed wind power to a measurable extent.

In scheduling strategies 3 and 4, which consider electrolyzer overload operation, there is reduced wind abandonment in the two typical working conditions owing to the increase in the upper operating limit of the electrolyzer, which enables it to directly absorb excess input wind power. In the strategy considering overloading of the electrolyzer, the power curve during the overloaded operation of the electrolyzer exhibits certain power fluctuations and wind curtailment phenomena., such as 0–5 h for Case 1 and 15–24 h for Case 2. This phenomenon is primarily attributed to the rapid increase in the internal temperature of the electrolyzer after more than 2 h of continuous overload operation, leading to the accelerated degradation of the electrolyzer, which may potentially result in equipment damage. Consequently, the power of the electrolyzer operation requires a reduction after 2 h of continuous operation to prevent equipment damage.

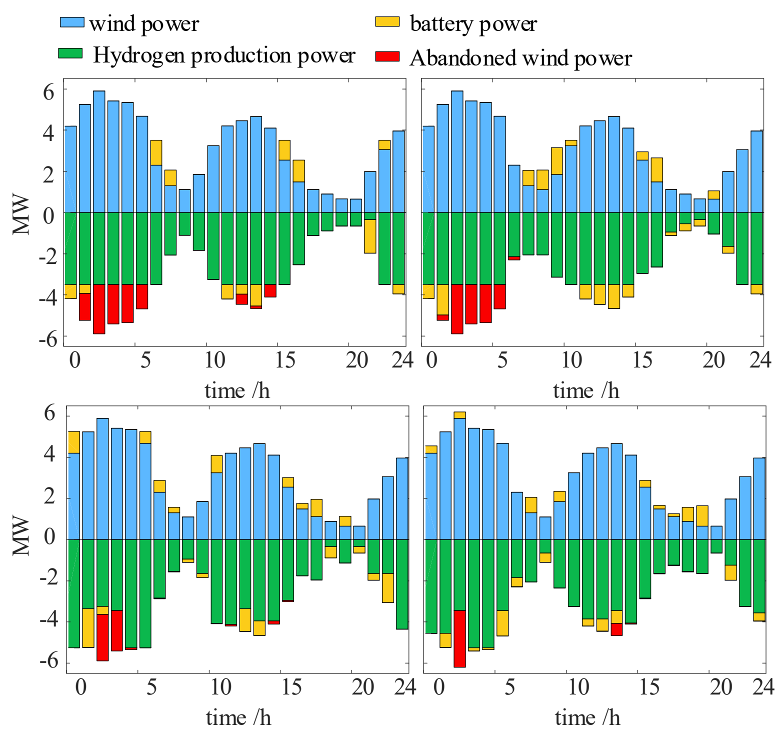


Working condition 1

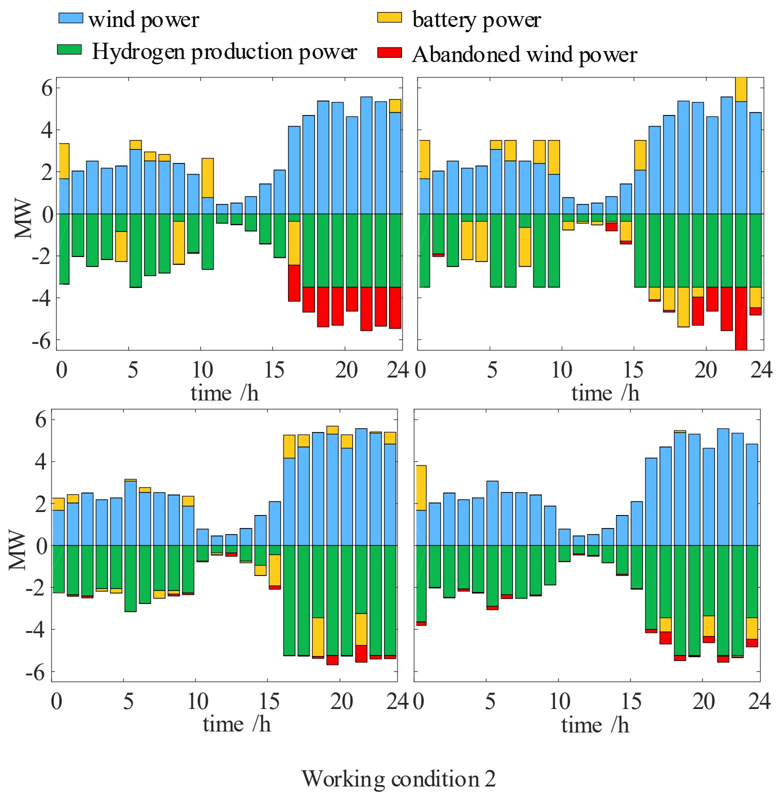


**Fig. 4.** Power allocation diagram for each device

When comparing Strategy 3 with Strategy 4, it is observed that Strategy 4 exhibits a lower electrolyzer overload intensity, as illustrated in Figure 5,10–15 h and 24 h for Case 1, and 16–24 h for Case 2. This phenomenon can be attributed to the consideration of the battery State of Charge (SOC) overrun, which is advantageous for enhancing the utilization capacity of energy storage batteries. Consequently, this approach reduces the operational demand for electrolyzer overload and extends the service life of electrolyzers.

In Case 2, Strategies 1 and 2 exhibit significant power fluctuations at certain intervals, potentially attributable to the fact that low-power operation is conducive to the reduction of membrane degradation, whereas minimal power fluctuation contributes to the reduction of catalyst degradation. Following the optimization to balance the extent of membrane degradation and catalyst degradation, the final optimization results for Strategies 1 and 2 were obtained.

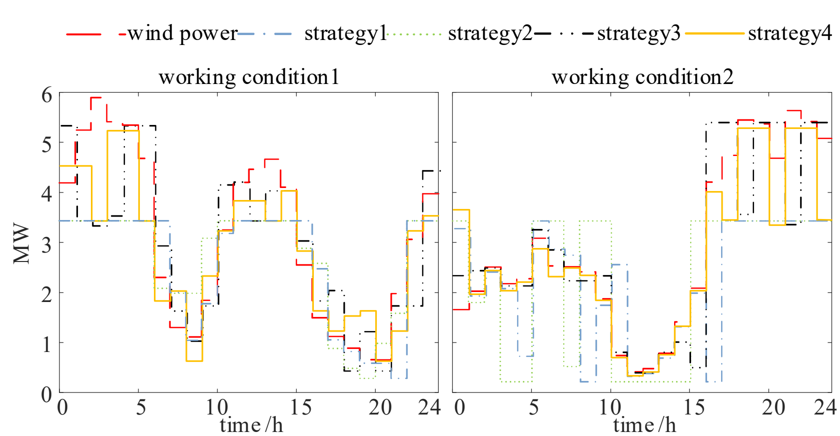


**Fig. 5.** Comparison chart of hydrogen production power for various strategies

A comparison of Strategy 2 with Strategy 4 reveals that Strategy 4 contributes to improving the capacity utilization of the battery and reducing the extent of battery degradation, as illustrated in Figure 6. Strategy 3 subjects the battery to overcharge and overdischarge from 0 to 10 h in case 1, from 0 to 5 h, and from 15 to 24 h in case 2, with the number of cycles and the cycle depth being significantly larger compared to strategy 4. Consequently, Strategy 4 is more effective in reducing the degradation cost of the battery and enhancing the economic efficiency of the system.

When strategies 1 and 3 are implemented, the State of Charge (SOC) of the energy storage battery is constrained between 0.2 and 0.8, resulting in partial utilization of the battery capacity. This limitation adversely affects the battery's peaking capability and capacity of the system to consume renewable energy.

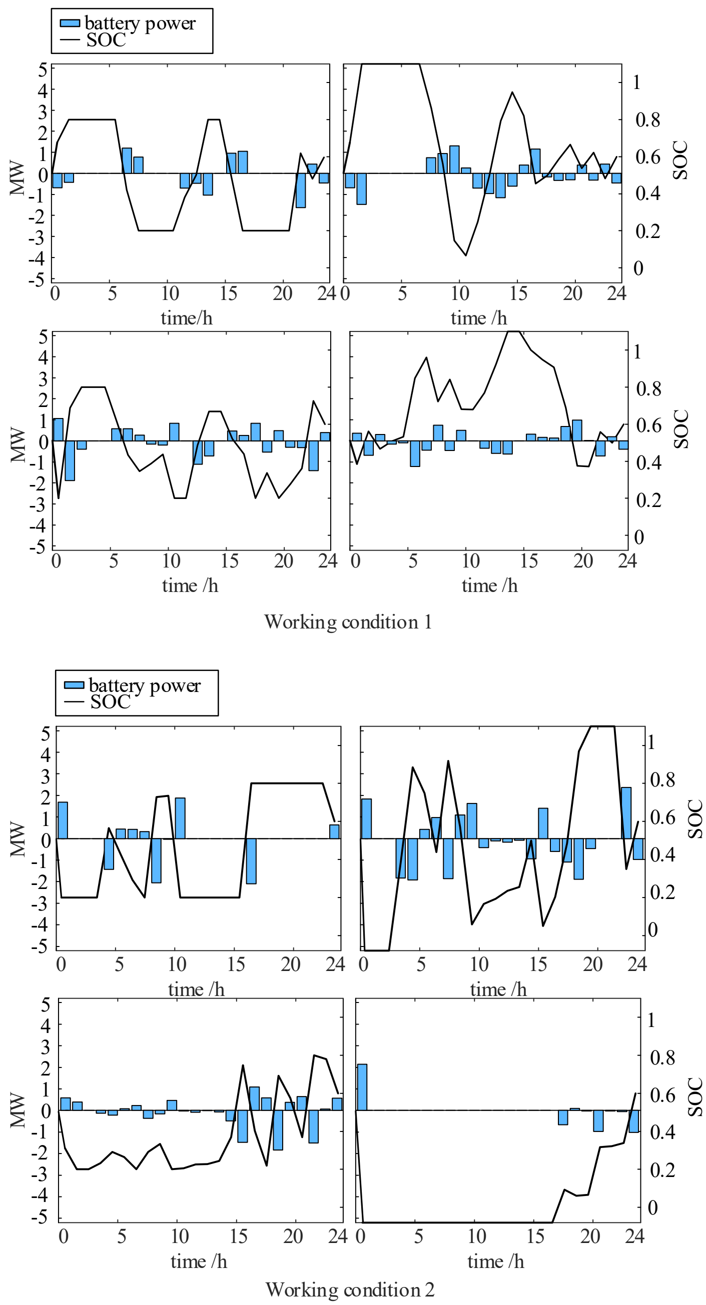


**Fig. 6.** Energy Storage Battery Power and SOC

To validate the superiority of the improved Mongoose optimization algorithm (ECPS-DMO) in addressing the optimization problem presented in this paper, comparative experiments were conducted using the Mongoose Algorithm (DMO), Whale Optimization Algorithm (WOA), and Beluga Whale Optimization Algorithm (BWO). The experiments were performed sequentially under typical operating conditions using the four algorithms; the resultant convergence curves are presented in Figure 7.

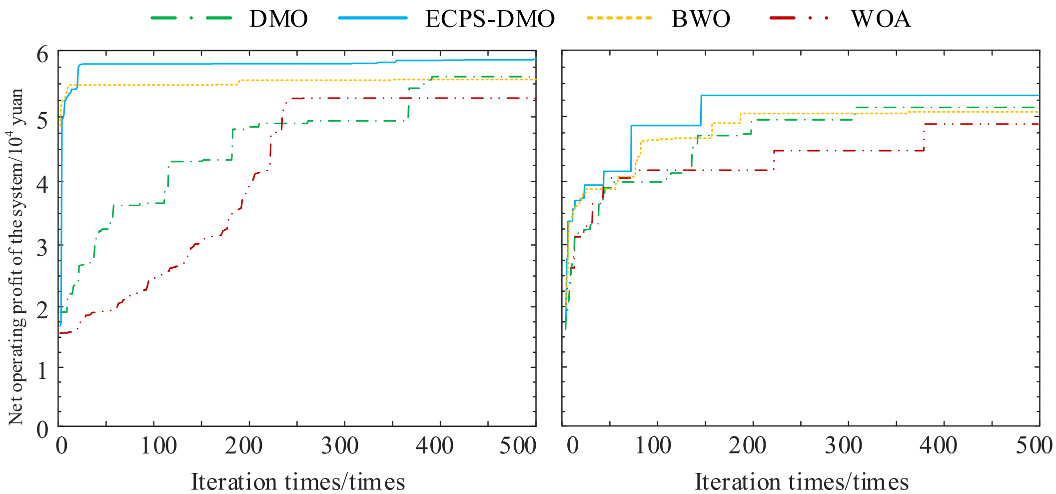


**Fig. 7.** Algorithm convergence curve

The ECPS-DMO algorithm demonstrates an effective balance between optimization quality and computational efficiency, exhibiting improved performance compared to the original DMO algorithm, as illustrated in Figure 7. The convergence values of the ECPS-DMO algorithm attain 5.77 × $10^4$ yuan and 5.44 × $10^4$ yuan for Case 1 and Case 2, respectively, indicating high optimization search accuracy. ECPS-DMO achieved convergence after 20 iterations for Case 1 and 150 iterations for Case 2, demonstrating a more rapid convergence. The rationale for this approach lies in the ECPS-DMO algorithm's incorporation of Latin hypercube sampling initialization to revise the convergence factor of the algorithm, which is integrated with the electrolyzer power-grading strategy to augment both the global search capability and the convergence rate of the algorithm.

The following factors were considered to assess system economics: battery degradation cost, electrolyzer degradation cost, wind abandonment cost, and hydrogen production revenue. Table 3 presents the evaluation indices for different strategies.

**Table 3.** Evaluation indicators for each strategy

| working condition | strategy | $C_{H2}$/yuan | $C_V$/yuan | $C_{Bd}$/yuan | $C_{loss}$/yuan | $f$/yuan |
|---|---|---|---|---|---|---|
| 1 | 1 | 64062.48 | 2182.31 | 2666.03 | 3450.19 | 55763.93 |
| | 2 | 65653.03 | 1939.16 | 3397.27 | 2713.13 | 57602.99 |
| | 3 | 69023.59 | 8708.20 | 2697.83 | 1437.52 | 56180.03 |
| | 4 | 70144.28 | 8483.51 | 2696.45 | 1225.28 | 57739.03 |
| 2 | 1 | 55692.25 | 1614.16 | 1702.60 | 4779.56 | 47595.91 |
| | 2 | 57032.84 | 1842.45 | 4095.83 | 3482.74 | 47611.81 |
| | 3 | 65959.91 | 10202.98 | 2285.48 | 854.37 | 52617.07 |
| | 4 | 66156.61 | 9172.72 | 1437.64 | 1050.91 | 54495.32 |

Under the two typical working conditions, optimal scheduling strategy 4 demonstrates superior economic performance, with net daily operating gains of 57,739.03yuan and 54,495.32yuan, respectively, as illustrated in Table 3. The economic advantage of strategy 4 is primarily attributed to the effective control of both the electrolyzer degradation cost and cell degradation cost. Compared to Strategy 2, Strategy 4 permits overloaded operation of the electrolyzer, resulting in a 20% reduction in battery degradation cost as opposed to 63%, a 54% decrease in the system's wind abandonment cost versus 69%, and a 6.8% increase in hydrogen production revenue compared to 15%. In contrast with Strategy 3, Strategy 4 allows the battery SOC to exceed its operational limit, leading to a 2.5% reduction in electrolyzer degradation cost versus 10.1% and a 1.6% increase in hydrogen production revenue as opposed to 0.29%. Consequently, Strategy 4 achieves optimal economic performance by enhancing hydrogen production gains and minimizing wind abandonment costs, while maintaining lower overall degradation costs.

A comprehensive evaluation of the indicators reveals that Strategy 4 effectively reduces the degradation of the energy storage battery and electrolyzer, while simultaneously increasing hydrogen production and reducing Wind power abandonment, as illustrated in Figure 8. The battery degradation in Strategy 4 for Case 1 is minimal, only marginally exceeding that of Strategy 1, whereas in Case 2, it demonstrates the least degradation, even lower than that of Strategy 1. This can be attributed to the fact that overloaded operation of the electrolyzer mitigates the peak pressure on the battery, thereby reducing battery degradation.

The electrolyzer degradation in Strategy 4 is more pronounced than that in Strategies 1 and 2 but less severe than that in Strategy 3. This phenomenon occurs because overloading of the electrolyzer results in increased degradation; however, expanding the utilized capacity of the battery enhances its peaking capability and reduces the duration of electrolyzer overloading, consequently diminishing electrolyzer degradation.

Strategy 4 exhibited the highest hydrogen production and the lowest wind curtailment. The wind curtailment in Case 2 exceeds that in Case 3, potentially because of the consideration of battery degradation costs, suggesting that curtailing this portion of wind energy is more economically advantageous for the system. The maintenance of hydrogen production levels in the system may be attributed to the relatively small amount of curtailed wind energy and the higher operating efficiency of the electrolyzer, which facilitates increased hydrogen production, even with reduced input power.

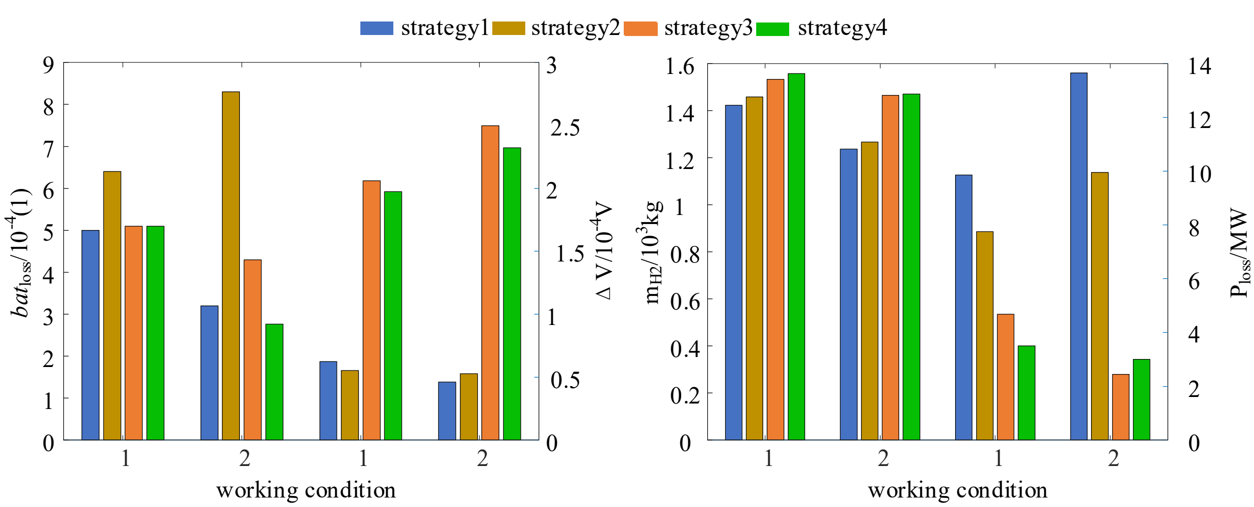


**Fig. 8.** Evaluation indicators for each strategy

## 6. Conclusions

This study proposes an optimized scheduling strategy for off-grid wind-power hydrogen production systems considering the degradation characteristics of electrolyzers and batteries. Through a comparative analysis of the system hydrogen production, electrolyzer voltage degradation, and battery degradation under typical operating conditions, the following conclusions were drawn.

1) Considering that the battery SOC exceeds the limit and electrolyzer overload operation, the utilization capacity of energy-storage batteries increases by approximately 96%, and the utilization capacity of electrolyzers increases by approximately 50%. These improvements contributed to the enhanced hydrogen production of the system and reduction in the wind curtailment rate. Consequently, the net operating profit of the system increases by approximately 3.6% and 14.5%, respectively.

2) The improved mongoose optimization algorithm (ECPS-DMO) proposed in this study enhances the computational efficiency and convergence accuracy of the algorithm by introducing Latin hypercube sampling initialization,modifying the convergence factor, and incorporating power-grading strategies. According to the example analysis, the computational efficiency of ECPS-DMO was improved by approximately 70% compared to traditional methods, and the convergence accuracy was improved by approximately 4%.

Subsequent research will further examine the impact of the efficiency variation characteristics of electrolyzers and the degradation characteristics of multiple electrolyzers on the optimized operation of the system. Additionally, an off-grid wind power hydrogen production system optimization model that considers the efficiency and degradation characteristics of electrolyzers was established.

## Author Contributions

Conceptualization, Z.L.; methodology, E.Z.; software, E.Z.; validation, E.Z.; formal analysis, X.X.; investigation, E.Z.; resources, Y.D.; data curation, E.Z.; writing—original draft preparation, E.Z.; writing—review and editing, X.C.; visualization, X.C.; supervision, C.Q.; project administration, Y.D.; funding acquisition, Z.L. All authors have read and agreed to the published version of the manuscript.

## Funding

This research received no external funding.

## Data Availability Statement

The data that support the findings of this study are available from the corresponding author upon reasonable request.

## Conflicts of Interest

The authors declare no conflict of interest.

## Disclaimer/Publisher's Note



## References

[1] Lakshmi, G. S., Rubanenko, O., Divya, G., & Lavanya, V. (2020, October). Distribution energy generation using renewable energy sources. In 2020 IEEE India Council International Subsections Conference (INDISCON) (pp. 108-113). IEEE.

[2] Blaabjerg, F., Yang, Y., Kim, K. A., & Rodriguez, J. (2023). Power electronics technology for large-scale renewable energy generation. Proceedings of the IEEE, 111(4), 335-355.

[3] Ho, W. S., Macchietto, S., Lim, J. S., Hashim, H., Muis, Z. A., & Liu, W. H. (2016). Optimal scheduling of energy storage for renewable energy distributed energy generation system. Renewable and Sustainable Energy Reviews, 58, 1100-1107.

[4] Kojima, H., Nagasawa, K., Todoroki, N., Ito, Y., Matsui, T., & Nakajima, R. (2023). Influence of renewable energy power fluctuations on water electrolysis for green hydrogen production. international journal of hydrogen energy, 48(12), 4572-4593.

[5] Han, L., Wang, S., Cheng, Y., Chen, S., & Wang, X. (2024). Multi-timescale scheduling of an integrated electric-hydrogen energy system with multiple types of electrolysis cells operating in concert with fuel cells. Energy, 307, 132707.

[6] Vargas-Ferrer, P., Álvarez-Miranda, E., Tenreiro, C., & Jalil-Vega, F. (2023). Integration of high levels of electrolytic hydrogen production: Impact on power systems planning. Journal of Cleaner Production, 409, 137110.

[7] Chau, K., Djire, A., & Khan, F. (2022). Review and analysis of the hydrogen production technologies from a safety perspective. International Journal of Hydrogen Energy, 47(29), 13990-14007.

[8] Abdin, Z., & Mérida, W. A. W. M. (2019). Hybrid energy systems for off-grid power supply and hydrogen production based on renewable energy: A techno-economic analysis. Energy Conversion and management, 196, 1068-1079.

[9] Al-Buraiki, A. S., & Al-Sharafi, A. (2022). Hydrogen production via using excess electric energy of an off-grid hybrid solar/wind system based on a novel performance indicator. Energy Conversion and Management, 254, 115270.

[10] Liang, T., Chai, L., Cao, X., Tan, J., Jing, Y., & Lv, L. (2024). Real-time optimization of large-scale hydrogen production systems using off-grid renewable energy: Scheduling strategy based on deep reinforcement learning. Renewable Energy, 224, 120177.

[11] Yang, G., Jiang, Y., & You, S. (2020). Planning and operation of a hydrogen supply chain network based on the off-grid wind-hydrogen coupling system. International Journal of Hydrogen Energy, 45(41), 20721-20739.

[12] Wang, Z., Jia, Y., Yang, Y., Cai, C., & Chen, Y. (2021). Optimal configuration of an off-grid hybrid wind-hydrogen energy system: Comparison of two systems. Energy Engineering, 118(6), 1641-1658.

[13] Sebbahi, S., Assila, A., Belghiti, A. A., Laasri, S., Kaya, S., Rachidi, S., & Hajjaji, A. (2024). A comprehensive review of recent advances in alkaline water electrolysis for hydrogen production. International Journal of Hydrogen Energy, 82, 583-599.

[14] Lange, H., Klose, A., Lippmann, W., & Urbas, L. (2023). Technical evaluation of the flexibility of water electrolysis systems to increase energy flexibility: A review. International Journal of Hydrogen Energy, 48(42), 15771-15783.

[15] Shi, T., Gu, L., Xu, Z., & Sheng, J. (2024). Research on Multi-Objective Energy Management of Renewable Energy Power Plant with Electrolytic Hydrogen Production. Processes, 12(3), 541.

[16] Zhang, Y., Zhang, T., Liu, S., Li, G., Zhang, Y., & Hu, Z. (2024). Multi-energy complementary optimal scheduling based on hydrogen gas turbine considering the flexibility of electrolyser. IET Renewable Power Generation, 18(12), 1972-1985.

[17] Zhang, L., Dai, W., Zhao, B., Zhang, X., Liu, M., Wu, Q., & Chen, J. (2023). Multi-time-scale economic scheduling method for electro-hydrogen integrated energy system based on day-ahead long-time-scale and intra-day MPC hierarchical rolling optimization. Frontiers in Energy Research, 11, 1132005.

[18] Li, Z., Xia, Y., Bo, Y., & Wei, W. (2024). Optimal planning for electricity-hydrogen integrated energy system considering multiple timescale operations and representative time-period selection. Applied Energy, 362, 122965.

[19] Petrollese, M., Valverde, L., Cocco, D., Cau, G., & Guerra, J. (2016). Real-time integration of optimal generation scheduling with MPC for the energy management of a renewable hydrogen-based microgrid. Applied Energy, 166, 96-106.

[20] Peng, W., Xu, Y., Li, G., Song, J., Xu, G., Xu, X., & Pan, Y. (2024). Research on typical operating conditions of hydrogen production system with off-grid wind power considering the characteristics of proton exchange membrane electrolysis cell. Global Energy Interconnection, 7(5), 642-652.

[21] Zhao, D., He, Q., Yu, J., Jiang, J., Li, X., & Ni, M. (2020). Dynamic behaviour and control strategy of high temperature proton exchange membrane electrolyzer cells (HT-PEMECs) for hydrogen production. International Journal of Hydrogen Energy, 45(51), 26613-26622.

[22] Guo, Y., Qi, P., Zhang, Q., Li, M., Liu, J., & Sun, H. (2025). Control strategy for hydrogen production system using HTO-based hybrid electrolyzers. Energy Reports, 13, 2354-2364.

[23] Fang, R., & Liang, Y. (2019). Control strategy of electrolyzer in a wind-hydrogen system considering the constraints of switching times. International journal of hydrogen energy, 44(46), 25104-25111.

[24] Wang, X., Meng, X., Nie, G., Li, B., Yang, H., & He, M. (2024). Optimization of hydrogen production in multi-Electrolyzer systems: A novel control strategy for enhanced renewable energy utilization and Electrolyzer lifespan. Applied Energy, 376, 124299.

[25] Li, Y., Deng, X., Zhang, T., Liu, S., Song, L., Yang, F., ... & Shen, X. (2023). Exploration of the configuration and operation rule of the multi-electrolyzers hybrid system of large-scale alkaline water hydrogen production system. Applied Energy, 331, 120413.

[26] Zheng, Y., Huang, C., Tan, J., You, S., Zong, Y., & Træholt, C. (2023). Off-grid wind/hydrogen systems with multi-electrolyzers: Optimized operational strategies. Energy Conversion and Management, 295, 117622.

[27] Huang, W., Zhang, B., Ge, L., He, J., Liao, W., & Ma, P. (2023). Day-ahead optimal scheduling strategy for electrolytic water to hydrogen production in zero-carbon parks type microgrid for optimal utilization of electrolyzer. Journal of Energy Storage, 68, 107653.

[28] Niu, M., Li, X., Sun, C., Xiu, X., Wang, Y., Hu, M., & Dong, H. (2023). Operation optimization of wind/battery storage/alkaline electrolyzer system considering dynamic hydrogen production efficiency. Energies, 16(17), 6132.

[29] Liang, T., Chen, M., Tan, J., Jing, Y., Lv, L., & Yang, W. (2024). Large-scale off-grid wind power hydrogen production multi-tank combination operation law and scheduling strategy taking into account alkaline electrolyzer characteristics. Renewable Energy, 232, 121122.